

The ESO Slice Project (ESP) galaxy redshift survey: *

II. The luminosity function and mean galaxy density

E.Zucca^{1,2}, G.Zamorani^{1,2}, G.Vettolani², A.Cappi¹, R.Merighi¹,
M.Mignoli¹, G.M.Stirpe¹, H.MacGillivray³, C.Collins⁴, C.Balkowski⁵, V.Cayatte⁵, S.Maurogordato⁵,
D.Proust⁵, G.Chincarini^{6,7}, L.Guzzo⁶, D.Maccagni⁸, R.Scaramella⁹, A.Blanchard¹⁰, and M.Ramella¹¹

¹ Osservatorio Astronomico di Bologna, via Zamboni 33, 40126 Bologna, Italy

² Istituto di Radioastronomia del CNR, via Gobetti 101, 40129 Bologna, Italy

³ Royal Observatory Edinburgh, Blackford Hill, Edinburgh EH9 3HJ, United Kingdom

⁴ School of EEEP, Liverpool John–Moores University, Byrom Street, Liverpool L3 3AF, United Kingdom

⁵ Observatoire de Paris, DAEC, Unité associée au CNRS, D0173 et à l'Université Paris 7, 5 Place J.Janssen, 92195 Meudon, France

⁶ Osservatorio Astronomico di Brera, via Bianchi 46, 22055 Merate (LC), Italy

⁷ Università degli Studi di Milano, via Celoria 16, 20133 Milano, Italy

⁸ Istituto di Fisica Cosmica e Tecnologie Relative, via Bassini 15, 20133 Milano, Italy

⁹ Osservatorio Astronomico di Roma, via Osservatorio 2, 00040 Monteporzio Catone (RM), Italy

¹⁰ Université L. Pasteur, Observatoire Astronomique, 11 rue de l'Université, 67000 Strasbourg, France

¹¹ Osservatorio Astronomico di Trieste, via Tiepolo 11, 34131 Trieste, Italy

Received 00 - 00 - 0000; accepted 00 - 00 - 0000

Abstract. The ESO Slice Project (ESP) is a galaxy redshift survey we have recently completed as an ESO Key–Project over about 23 square degrees, in a region near the South Galactic Pole. The survey is nearly complete to the limiting magnitude $b_J = 19.4$ and consists of 3342 galaxies with reliable redshift determination.

The ESP survey is intermediate between shallow, wide angle samples and very deep, one–dimensional pencil beams: spanning a volume of $\sim 5 \times 10^4 h^{-3} \text{ Mpc}^3$ at the sensitivity peak ($z \sim 0.1$), it provides an accurate determination of the “local” luminosity function and the mean galaxy density.

We find that, although a Schechter function (with $\alpha = -1.22$, $M_{b_J}^* = -19.61 + 5 \log h$ and $\phi^* = 0.020 h^3 \text{ Mpc}^{-3}$) is an acceptable representation of the luminosity function over the entire range of magnitudes ($M_{b_J} \leq -12.4 + 5 \log h$), our data suggest the presence of a steepening of the luminosity function for $M_{b_J} \geq -17 + 5 \log h$. Such a steepening at the faint end of the luminosity function, well fitted by a power law with slope $\beta \sim -1.6$, is almost completely due to galaxies with emission lines: in fact, dividing our galaxies into two samples, i.e. galaxies with and without emission lines, we find significant differ-

ences in their luminosity functions. In particular, galaxies with emission lines show a significantly steeper slope and a fainter M^* .

The amplitude and the α and M^* parameters of our luminosity function are in good agreement with those of the AUTOFIB redshift survey (Ellis et al. 1996). Viceversa, our amplitude is significantly higher, by a factor ~ 1.6 at $M \sim M^*$, than that found for both the Stromlo-APM (Loveday et al. 1992) and the Las Campanas (Lin et al. 1996) redshift surveys. Also the faint end slope of our luminosity function is significantly steeper than that found in these two surveys.

The galaxy number density for $M_{b_J} \leq -16 + 5 \log h$ is well determined ($\bar{n} = 0.08 \pm 0.015 h^3 \text{ Mpc}^{-3}$). Its estimate for $M_{b_J} \leq -12.4 + 5 \log h$ is more uncertain, ranging from $\bar{n} = 0.28 h^3 \text{ Mpc}^{-3}$, in the case of a fit with a single Schechter function, to $\bar{n} = 0.54 h^3 \text{ Mpc}^{-3}$, in the case of a fit with a Schechter function and a power law. The corresponding blue luminosity densities in these three cases are $\rho_{LUM} = (2.0, 2.2, 2.3) \times 10^8 h \text{ L}_\odot \text{ Mpc}^{-3}$, respectively. Large over- and under- densities are clearly seen in our data. In particular, we find evidence for a “local” under-density ($n \sim 0.5\bar{n}$ for $D_{comoving} \leq 140 h^{-1} \text{ Mpc}$) and a significant overdensity ($n \sim 2\bar{n}$) at $z \sim 0.1$. When these radial density variations are taken into account, our derived luminosity function reproduces very well the ob-

Send offprint requests to: Elena Zucca (zucca@astbo1.bo.cnr.it)

* based on observations collected at the European Southern Observatory, La Silla, Chile.

served counts for $b_J \leq 19.4$, including the steeper than Euclidean slope for $b_J \leq 17.0$.

Key words: Galaxies: distances and redshifts - luminosity function - density

1. Introduction

An unbiased and detailed characterization of the luminosity function of field galaxies is a basic requirement in many extragalactic problems. Although several determinations of this function are already available in the literature, the debate about the faint end slope and the normalization of the luminosity function is still open. These quantities allow a “local” normalization which is crucial for the study of galaxy evolution and for the explanation of the faint galaxy counts.

Wide angle, shallow samples such as CfA2 ($m_Z \leq 15.5$, Marzke et al. 1994), SSRS2 ($m_{B(0)} \leq 15.5$, da Costa et al. 1994, Marzke & da Costa 1997) and Stromlo-APM ($b_J \leq 17.15$, Loveday et al. 1992) surveys, can provide good determinations of the shape of the luminosity function both globally and for different morphological types, but the normalization can in principle be significantly affected by local fluctuations.

Very deep samples, such as the AUTOFIB composite survey ($b_J \leq 24$, Ellis et al. 1996) and the CFHT redshift survey ($17.5 < I_{AB} < 22.5$, Lilly et al. 1995), are mainly designed to study evolutionary effects in the luminosity function.

The ESO Slice Project (ESP, $b_J \leq 19.4$, Vettolani et al. 1997a) is aimed to fill the gap between shallow, wide angle surveys and very deep, one-dimensional pencil beams, allowing a robust estimate of the faint end slope and normalization of the luminosity function derived from a large, uniform and complete sample of galaxies. The redshift distribution of the galaxies of this sample, which peaks at $z \sim 0.1$, is deep enough to allow the sampling of a statistically representative distribution of the structures in a region of the Universe where the evolutionary effects are not expected to be important.

The recently published Las Campanas Redshift Survey (LCRS, $r \lesssim 17.5$, Lin et al. 1996), based on a large number of galaxies with redshift ($N_{gal} \sim 19000$), probes essentially the same redshift depth as the ESP survey, but on a larger solid angle. The main differences between the LCRS and our survey, as well as most of the existing surveys, are the photometric band in which the galaxies have been selected (red instead of blue) and the fact that the low surface brightness galaxies have been deliberately excluded from the spectroscopic sample (Shectman et al. 1996). These facts can make somewhat difficult a direct comparison between the LCRS luminosity function and others, including ours.

The organization of the paper is as follows. In Sect.2 we briefly summarize the characteristics of the ESP galaxy redshift survey and in Sect.3 we deal with the problem of the K-correction. In Sect.4 and 5 we describe the methods of derivation and the results for the luminosity function and the mean galaxy density, respectively. In Sect.6 we discuss our results and compare them with previous estimates of the luminosity function. In Sect.7 we summarize our results.

2. The ESO Slice Project

The ESO Slice Project (ESP) galaxy redshift survey is described in Vettolani et al. (1997a, hereafter paper I) and all the data for the sample will be published in Vettolani et al. (1997b, hereafter paper III): here we summarize only the main characteristics of the survey.

The ESP survey extends over a strip of $\alpha \times \delta = 22^\circ \times 1^\circ$, plus a nearby area of $5^\circ \times 1^\circ$, five degrees west of the main strip, in the South Galactic Pole region. The position was chosen in order to minimize the galactic absorption effects ($-60^\circ \lesssim b^{II} \lesssim -75^\circ$). The target objects, with a limiting magnitude $b_J \leq 19.4$, were selected from the Edinburgh-Durham Southern Galaxy Catalogue (EDSGC, Heydon-Dumbleton et al. 1988).

The right ascension limits are 22^h30^m and 01^h20^m , at a mean declination of $-40^\circ15'$ (1950). We have covered this region with a regular grid of adjacent circular fields, with a diameter of 32 arcmin each, corresponding to the field of view of the multifiber spectrograph OPTOPUS (Lund 1986) at the 3.6m ESO telescope. The total solid angle of the spectroscopic survey is 23.2 square degrees. In order to increase the overall completeness, in the last observing run we have used the MEFOS spectrograph (Felenbok et al. 1997), which has a larger field of view but a smaller number of fibers, to observe some of the objects which either had not been observed in the OPTOPUS observing runs or for which only poor quality spectra were available. We observed a total of 4044 objects, corresponding to $\sim 90\%$ of the parent photometric sample, which contains 4487 objects: the objects we observed were selected to be a random subset of the total catalogue with respect to both magnitude and surface brightness. The total number of confirmed galaxies with reliable redshift measurement is 3342, while 493 objects turned out to be stars and 1 object is a quasar at redshift $z \sim 1.174$. No redshift measurement could be obtained for the remaining 208 spectra. All the details about data reduction, number of objects and completeness of the sample are reported in paper I and paper III.

The volume of the survey is $\sim 5 \times 10^4 h^{-3} \text{ Mpc}^3$ at $z \sim 0.1$, corresponding to the sensitivity peak of the survey, and $\sim 1.9 \times 10^5 h^{-3} \text{ Mpc}^3$ at $z \sim 0.16$, corresponding to the effective depth of the sample.

The absolute magnitudes are computed as

$$M = m - 25 - 5 \log D_L(z) - K(z) \quad (1)$$

where the luminosity distance D_L is given by the Matig (1958) expression (throughout the paper we adopt $H_o = 100$ km/s Mpc $^{-1}$ and $q_o = 0.5$) and $K(z)$ is the K-correction. The galactic absorption is assumed to be negligible, because the strip is close to the South Galactic Pole (Fong et al. 1987).

Finally, we note that the median internal velocity error for our galaxies (~ 60 km/s) is quite small compared to the survey depth, and therefore its effect on the calculation of absolute magnitudes can be neglected.

3. The K-correction

Since our database was selected in the blue-green band, K-corrections are needed to compute the luminosity function even for the moderate redshifts sampled by our galaxies ($z \leq 0.3$). The application of the functional forms of the K-correction as a function of redshift (e.g. Shanks et al. 1984) obviously requires the knowledge of the morphological type of each galaxy, which is not available for most of our galaxies. We are currently refining a procedure to estimate the K-correction for each galaxy directly from the spectra, but this work is still in progress. Therefore, for this paper we have adopted the following statistical approach.

mix at each redshift. This average K-correction is defined as

$$\langle K(z) \rangle = \sum_i f_i(z) K_i(z) \quad (2)$$

where $f_i(z)$ is the fraction of galaxies of the i^{th} morphological type, at redshift z , whose K-correction is $K_i(z)$. The expected fractions of each morphological type, as well as their K-corrections, have been computed using the Pozzetti et al. (1996) pure luminosity evolution model. This model, based on the galaxy spectral library of Bruzual & Charlot (1993), is constrained to match the empirical K-corrections and the morphological mix derived locally, and at our moderate redshift the results are almost independent of the details of the adopted evolutionary model. In Fig.1 we show our “weighted” K-correction, computed in bins of 0.025 in redshift (solid circles), with a polynomial fit superimposed on the points (solid line). The decrease of $K(z)$ for $z \geq 0.2$ is essentially due to the fact that the expected fraction of early-type galaxies, which have a larger K-correction, becomes smaller at this redshift, while the fraction of bluer galaxies with smaller or almost zero K-correction increases.

Each galaxy at redshift z' is therefore assigned this “weighted” K-correction when computing its absolute magnitude. In the non-parametric derivation of the luminosity function (see Sect.4.1) we compute for each galaxy the maximum redshift within which it would still be included in the sample (z_{max}). For this purpose the K-correction for $z' \leq z \leq z_{max}$ is computed by keeping constant the morphological mix at the value corresponding to the measured redshift z' . In this way the K-correction at z_{max} can be written as:

$$\langle K(z_{max}) \rangle = \sum_i f_i(z') K_i(z_{max}) \quad (3)$$

4. The luminosity function

4.1. The method

For most samples of field galaxies the luminosity function is well represented by a Schechter (1976) form

$$\phi(L, x, y, z) dL dV = \phi^* \left(\frac{L}{L^*} \right)^\alpha e^{-L/L^*} d \left(\frac{L}{L^*} \right) dV \quad (4)$$

where α and L^* are parameters referring to the shape of the function and ϕ^* contains the information about the normalization; these parameters have to be determined from the data.

Many different methods have been used in the past years to compute the parameters of the galaxy luminosity function. Recently, however, the STY method (Sandage et al. 1979) has been the most widely used, and it has been shown that it is unbiased with respect to density inhomogeneities (see for instance Efstathiou et al. 1988, Bardelli

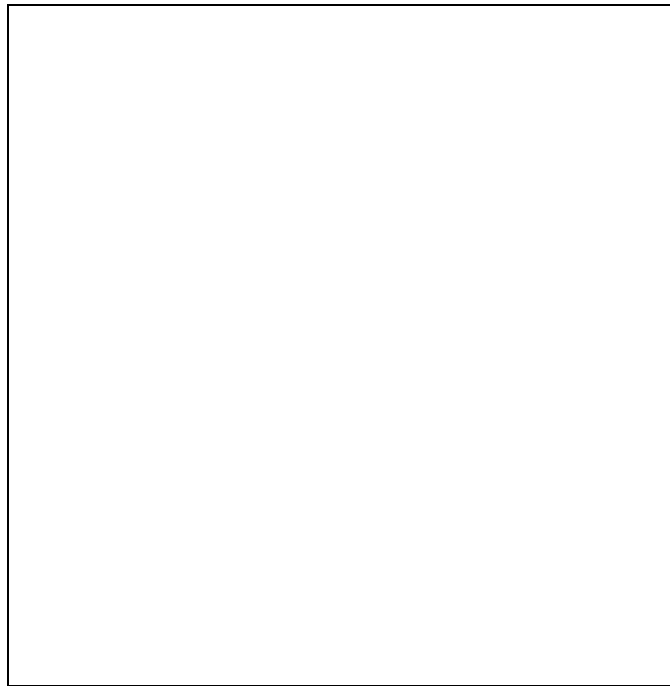


Fig. 1. Adopted weighted K-correction as a function of redshift. The solid line is a polynomial fit to the points.

We have computed an average K-correction, as a function of redshift, “weighted” with the expected morphological

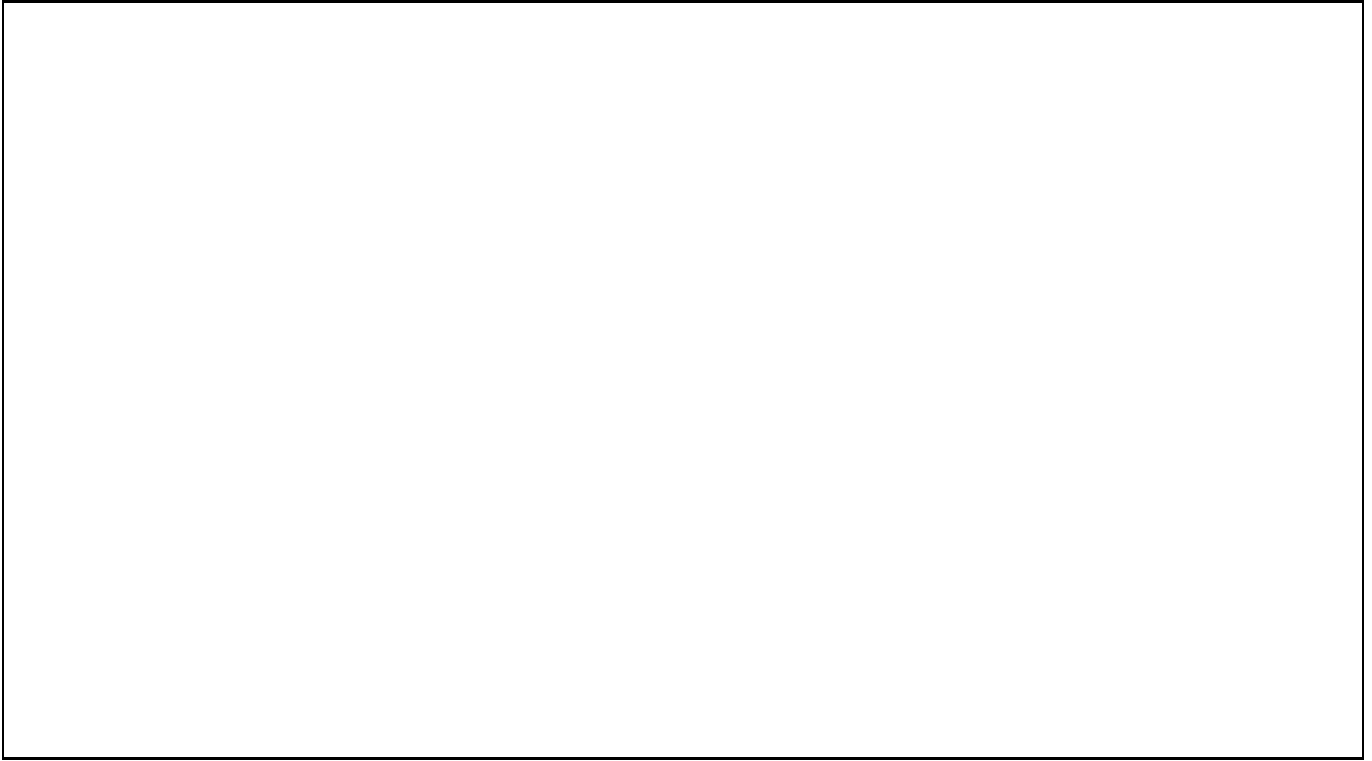


Fig. 2. a) Normalized luminosity function for 3342 ESP galaxies brighter than $M_{b_j} = -12.4 + 5 \log h$. The solid circles are computed with a modified version of the C-method (error bars represent 1σ Poissonian uncertainties), while the fits are obtained with the STY method. Dashed line: single Schechter function; solid line: Schechter function and power law. b) The same as panel a), but for galaxies with (open squares and dashed line) and without (filled squares and dotted line) emission lines. For clarity only the fit with Schechter function and power law is shown.

et al. 1991). The basic idea of this method is to compute the estimator of the quantity $\frac{\phi}{\Phi}$, where Φ is the integral luminosity function. Under the assumption that the shape of the luminosity function is not a function of position [i.e. $\phi(L, x, y, z) dL dV = \rho(x, y, z) dV \psi(L) dL$], the probability of seeing a galaxy of luminosity L_i at redshift z_i is

$$p_i = \frac{\psi(L_i)}{\int_{L_{min}(z_i)}^{+\infty} \psi(L) dL} \quad (5)$$

where $L_{min}(z_i)$ is the minimum luminosity observable at redshift z_i in a magnitude-limited sample.

The best parameters α and L^* of the luminosity function are then determined by maximizing the likelihood function $\mathcal{L}(\alpha, L^*)$, which is the product over all the galaxies of the individual probabilities p_i . This corresponds to minimize the function

$$\mathcal{S} = -2 \ln \mathcal{L} = -2 \left[\alpha \sum_{i=1}^N \ln L_i - N(\alpha + 1) \ln L^* - \frac{1}{L^*} \sum_{i=1}^N L_i - \sum_{i=1}^N \ln \Gamma \left(\alpha + 1, \frac{L_{min}(z_i)}{L^*} \right) \right] \quad (6)$$

where Γ is the incomplete Euler gamma function and N is the total number of galaxies in the sample.

The normalization parameter ϕ^* is not determined from these equations, and will be derived from the mean galaxy density in Sect.5.

The STY method is parametric, i.e. it assumes a shape for the luminosity function: the derived fit can be compared with the results of a non-parametric method based on the same assumptions. We use a modified version of the C-method of Lynden-Bell (1971): given a galaxy of luminosity L_i at redshift z_i its contribution to the luminosity function can be estimated as

$$\psi(L_i) = \frac{1 - \sum_{k=1}^{i-1} \psi(L_k)}{C^+(L_i)} \quad (7)$$

where $C^+(L_i)$ is the number of galaxies with luminosity $L \geq L_i$ and redshift $z \leq z_{max}(L_i)$. The resulting integral function $\sum_i \psi(L_i)$ is normalized to unity at the minimum luminosity of the sample. The quantity $\psi(L_i)$ is computed for each galaxy and the results are binned in luminosity bins and compared with the Schechter function derived with the STY method.

Table 1. Parameters of the luminosity function

Sample	M_{min}	N_{gal}	α	$M_{b,J}^*$	$\phi^* (h^3 \text{ Mpc}^{-3})$	β	M_c
Galaxies in the total sample	-12.4	3342	$-1.22^{+0.06}_{-0.07}$	$-19.61^{+0.06}_{-0.08}$	0.020 ± 0.004		
	-12.4	3342	-1.16	-19.57	0.021	-1.57	-16.99
Galaxies with emission lines	-12.4	1575	$-1.40^{+0.09}_{-0.10}$	$-19.47^{+0.10}_{-0.11}$	0.010 ± 0.002		
	-12.4	1575	-1.34	-19.42	0.010	-1.70	-16.94
Galaxies without emission lines	-12.4	1767	$-0.98^{+0.09}_{-0.09}$	$-19.62^{+0.08}_{-0.10}$	0.011 ± 0.002		
	-12.4	1767	-0.90	-19.57	0.012	-1.38	-17.22

4.2. The results

The normalized Schechter luminosity function derived with the STY method is shown in Fig.2a (dashed line) together with the data points obtained with the non-parametric C-method. The error bars on these points correspond to the statistical (i.e. Poissonian) errors. While the Schechter function is an excellent representation of the C-method data points for $M_{b,J} \lesssim -16 + 5 \log h$, at fainter magnitudes it lies below all the points down to $M_{b,J} = -12.4 + 5 \log h$. We have therefore modified the model function, adopting a Schechter function for $L > L_c$ and a power law for $L \leq L_c$. In this case the low luminosity part of the luminosity function is described by:

$$\psi(L)dL = A^* \left(\frac{L}{L^*} \right)^\beta d \left(\frac{L}{L^*} \right) \quad (8)$$

with β and L_c being two additional free parameters in the fitting procedure, while the normalization A^* is fixed by requiring continuity of the two functions at $L = L_c$.

The fit with this two-law function (solid line in Fig.2a) is almost indistinguishable from the single Schechter function at bright magnitudes, and reproduces very well also the faint part of the luminosity function. Statistically, as judged from the decrease of the \mathcal{S} function, the improvement of the two-law fit with respect to a single Schechter function is significant at about 2σ level, and we can therefore conclude that our data suggest the presence of a steepening of the luminosity function for $M_{b,J} \gtrsim -17 + 5 \log h$. In our sample there are 134 galaxies with $M_{b,J} \geq -17 + 5 \log h$ and 38 galaxies with $M_{b,J} \geq -16 + 5 \log h$: the sampled volumes are $\sim 1.4 \times 10^4 h^{-3} \text{ Mpc}^3$ for galaxies with $M_{b,J} = -17 + 5 \log h$ and $\sim 3.7 \times 10^3 h^{-3} \text{ Mpc}^3$ for galaxies with $M_{b,J} = -16 + 5 \log h$.

The derived best fit parameters are listed in the first two lines of Table 1. The errors given for the case of a single Schechter function are the projections onto the α and $M_{b,J}^*$

axes of the 1σ confidence ellipse (see Fig.3a) for two interesting parameters ($\Delta\mathcal{S} = 2.30$).

The errors for the two-law function are not reported in the table because, given the intrinsic correlations among the four fitted parameters, it is not very meaningful to give the projection on the four axes of the global four-dimensional error volume. However, we analyzed all the possible combinations of pairs of parameters, considering in turn each pair as “interesting” parameters (Avni 1976). From this analysis we find that the errors in α and M^* are very similar to, although slightly larger than, those computed for the case of a single Schechter function, while M_c is not well constrained by the data, with a 1σ error larger than one magnitude.

Fig.3b shows the 2σ contours in the (α, β) plane, which is the most relevant one in determining the reality of the steepening at low luminosity. Note that no point of the dotted line, corresponding to the locus $\alpha = \beta$ (i.e. no steepening) is within the allowed region.

The faint end steepening is almost completely due to galaxies with detectable emission lines. In fact, dividing the galaxies into two samples, i.e. galaxies with and without emission lines (1575 and 1767 galaxies respectively), we find very significant differences in their luminosity functions. Note that, given the typical signal to noise ratio of our spectra, detection of a line implies an equivalent width larger than about 5 \AA . Fig.2b shows the normalized luminosity functions for galaxies with (open squares and dashed line) and without emission lines (solid squares and dotted line): for clarity only the fit for the two-law function (Schechter function and power law at low luminosity) is plotted. It is clearly seen from the figure that galaxies with emission lines show a significantly steeper faint end slope and a slightly fainter M^* (see best fit parameters in Table 1). The volume density of galaxies with emission lines is lower than the volume density of galaxies without emission lines at bright magnitudes, but becomes

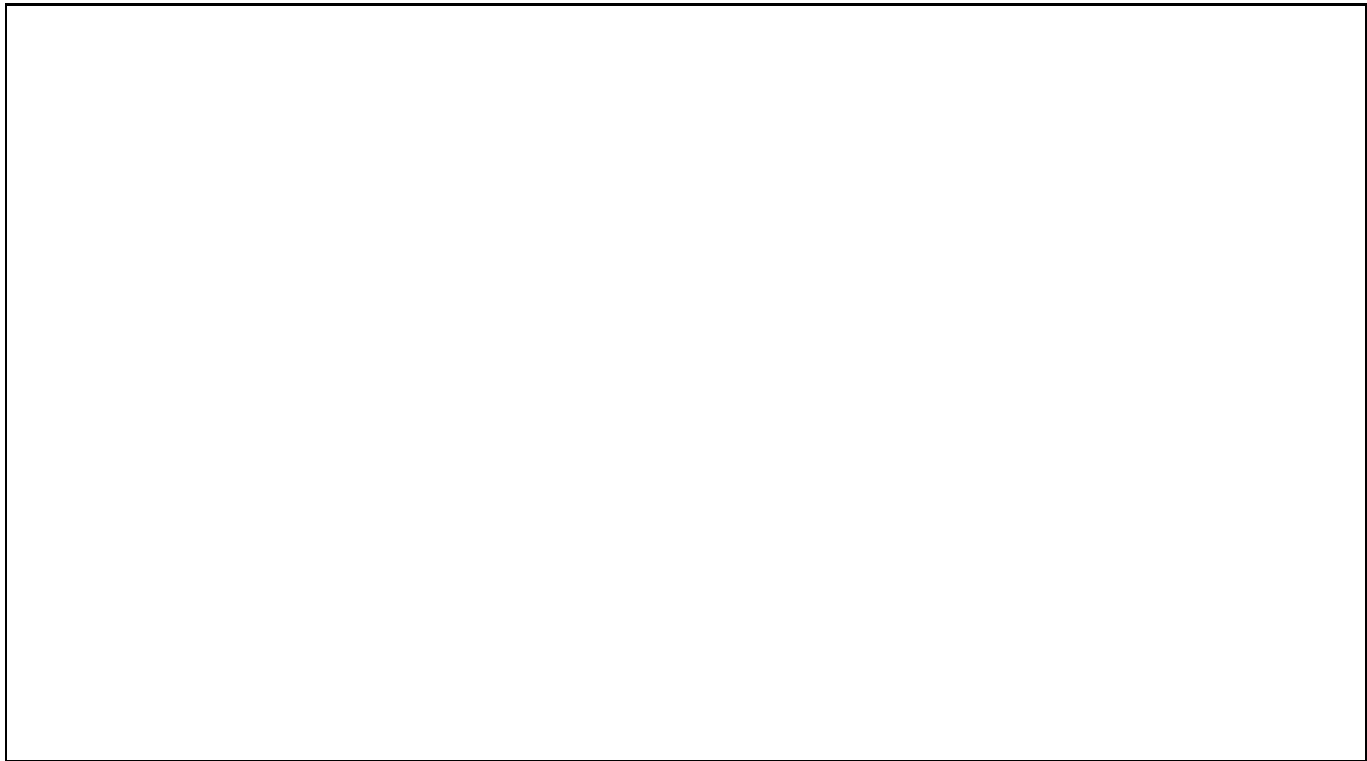


Fig. 3. a) Confidence ellipses at 1σ and 2σ levels for the parameters α and M^* , in the case of a fit with a single Schechter function, for the total sample and for galaxies with and without emission lines. b) Confidence ellipse at 2σ level in the (α, β) plane, in the case of a fit with Schechter function and power law for the total sample. The dotted line corresponds to the locus $\alpha = \beta$.

higher at faint magnitudes. The difference between the luminosity functions of galaxies with and without emission lines was noted quite early in the project (see for instance Vettolani et al. 1992), when only a fraction of the redshifts was available. Fig.3a, which shows the 1σ and 2σ confidence ellipses of the parameters α and M^* (single Schechter function case) for the total sample and for galaxies with and without emission lines, clearly demonstrates that the difference between the two subsamples is highly significant.

A similar difference in the best fit parameters of galaxies with and without emission lines has been found in the LCRS (see Fig.10 in Lin et al. 1996), although for each subsample their best fit slope is significantly flatter than the corresponding slope in our survey.

Finally, in order to check the possible existence of evolutionary effects also at our moderate redshifts, we have divided the ESP galaxies in three comoving distance bins, chosen in order to have three samples with a comparable number of objects ($D_{com} \leq 250 h^{-1}$ Mpc ; $250 h^{-1}$ Mpc $< D_{com} \leq 360 h^{-1}$ Mpc ; $D_{com} > 360 h^{-1}$ Mpc). The 1σ confidence ellipses of the (α, M^*) parameters for the three derived luminosity functions are reported in Fig.4. From the overlap of the ellipses we can say that no evidence for evolution is seen in our data, in agreement

with the conclusion of Ellis et al. (1996) that the bulk of the evolution sets in beyond $z \sim 0.3$.

As a final check, in order to estimate the maximum amount of uncertainty induced by our use of a statistical K-correction, we have also computed the parameters of the luminosity function with the two extreme assumptions that all galaxies are either ellipticals or spirals. Even in these cases, the derived parameters are not much different from those listed in Table 1. The maximum variations are $\Delta\alpha \sim -0.06$ (i.e. steeper slope) and $\Delta M^* \sim -0.22$ (i.e. brighter M^*) when we apply to all galaxies the K-correction appropriate for elliptical galaxies. Moreover, in both cases the difference between the parameters for galaxies with and without emission lines remains highly significant.

4.3. The influence of magnitude errors and redshift incompleteness.

The observed luminosity function is a convolution of the true luminosity function with the magnitude error distribution (Efstathiou et al. 1988). Assuming that the distribution of the magnitude errors is Gaussian, with dispersion σ_M (independent of m), the observed luminosity



Fig. 4. Confidence ellipses at 1σ level for the parameters α and M^* of the luminosity functions in three different distance bins. The asterisk refers to the best fit parameters for the total sample.

function ϕ_{obs} is related to the true luminosity function ϕ_{true} as

$$\phi_{obs}(M) = \frac{1}{\sqrt{2\pi}\sigma_M} \int_{-\infty}^{+\infty} \phi_{true}(M') e^{-(M'-M)^2/2\sigma_M^2} dM' \quad (9)$$

Preliminary analysis of CCD data in our survey area for about 80 galaxies in the magnitude range $16.5 \leq b_J \leq 19.4$ shows a linear relation between $b_J(EDSGC)$ and $m_B(CCD)$ over the entire range of magnitude, with a dispersion (σ_M) of about 0.2 magnitudes around the fit (Garilli et al. in preparation). Since the CCD pointings cover the entire right ascension range of our survey, this σ_M includes both statistical errors within single plates and possible plate-to-plate zero point variations. With the conservative assumption that the observed $\sigma_M = 0.2$ is entirely due to errors on EDSGC magnitudes, we have computed the parameters for the case of a Schechter function using the convolved luminosity function of eq.(9) in the likelihood function. The resulting best fit parameters are very similar to those shown in Table 1, with the slope α becoming flatter by ~ 0.05 and M^* fainter by ~ 0.10 . Even more negligible are the effects on the best fit parameters of our small redshift incompleteness. Eq.(5) is correct only for a complete, unbiased sample in which all galaxies with $m < m_{lim}$ are members of the sample or all galaxies with $m < m_{lim}$ have the same probability of being members of the sample (as, for example, in a redshift

survey with $1/n$ sampling). If this is not the case, it has been shown by Zucca et al. (1994) that eqs.(5) and (6) have to be modified as:

$$p_i = \left(\frac{\psi(L_i)}{\int_{L_{min}(z_i)}^{+\infty} \psi(L) dL} \right)^{w_i} \quad (10)$$

and

$$S = -2 \left[\alpha \sum_{i=1}^N w_i \ln L_i - (\alpha + 1) \ln L^* \sum_{i=1}^N w_i - \frac{1}{L^*} \sum_{i=1}^N w_i L_i - \sum_{i=1}^N w_i \ln \Gamma \left(\alpha + 1, \frac{L_{min}(z_i)}{L^*} \right) \right] \quad (11)$$

where w_i is the inverse of the probability that the i^{th} galaxy has of being included in the sample.

For the ESP sample there are two kinds of redshift incompleteness: objects which have not been observed and objects whose spectra were not useful for redshift determination. We have verified that the former incompleteness ($\sim 10\%$) is consistent with being random in magnitude. As such, it does not affect the derived parameters α and M^* , but has to be taken into account when determining the luminosity function normalization (see next section). On the other hand, the latter incompleteness ($\sim 5\%$) is higher for fainter objects and is well described by:

$$f(m) = \begin{cases} 0 & \text{if } m \leq 16.2 \\ 0.023(m - 16.2) & \text{if } m > 16.2 \end{cases} \quad (12)$$

Note that the maximum fraction of galaxies for which the spectra did not provide a useful z determination is $\sim 7\%$ for the faintest galaxies of our survey ($b_J = 19.4$), for which the corresponding weight $w_i = 1/[1 - f(m_i)]$ is 1.08. Applying this correction to ESP galaxies, we find that the effect on the best fit parameters are completely negligible, i.e. $\Delta\alpha \sim \Delta\beta \sim -0.02$, $\Delta M^* \sim \Delta M_c \sim 0.01$.

5. The mean galaxy density

5.1. The method

Given a magnitude limited sample, an unbiased estimator for the mean number density of galaxies \bar{n} is

$$\bar{n} = \frac{\sum_i n_i W(z_i)}{\int F(z) W(z) \frac{dV}{dz} dz} \quad (13)$$

where $W(z)$ is a weighting function and $F(z)$ is the selection function of the sample, defined as

$$F(z) = \frac{\int_{\max[L_1, L_{min}(z)]}^{+\infty} \phi(L) dL}{\int_{L_1}^{+\infty} \phi(L) dL} \quad (14)$$

where L_1 is the minimum luminosity considered in the estimate of the luminosity function. The selection function represents the ratio between the number of galaxies detectable at redshift z and the total number of galaxies with $L \geq L_1$ at the same redshift. Davis & Huchra (1982; DH82) have discussed a number of different estimators for \bar{n} , corresponding to different choices for the weighting function $W(z)$, and have shown that the minimum variance estimator is n_{J_3} , obtained with $W(z_i) = 1/[1 + \bar{n}J_3F(z_i)]$, where J_3 is the second moment of the spatial correlation function $\xi(r)$. Adopting $J_3 \sim 10,000$, as found from a fit of the correlation function in various surveys (see for instance Stromlo-APM and LCRS), including ours, and using the formula given in the appendix of DH82, we find that the expected fractional error on \bar{n} is $\sim 10\%$. Note, however, that this error estimate accounts only for the part due to galaxy clustering and does not take into account the additional uncertainty arising from the errors on the parameters of the luminosity function. By varying α and M^* along their 1σ confidence ellipse, we find that the errors on \bar{n} induced by the uncertainty on the parameters of the luminosity function are significantly larger ($\sim 20\%$) than those due to galaxy clustering. Therefore, since there is no a priori reason to prefer the n_{J_3} estimator with respect to other possible estimators, we have analyzed the behaviour of all the estimators discussed by DH82.

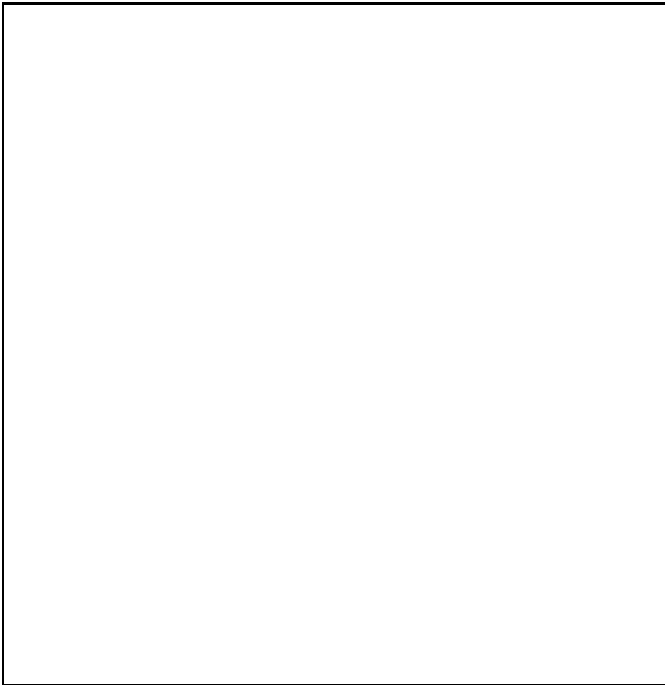


Fig. 5. Integrated average density as a function of the maximum comoving distance for the four DH82 estimators (see text).

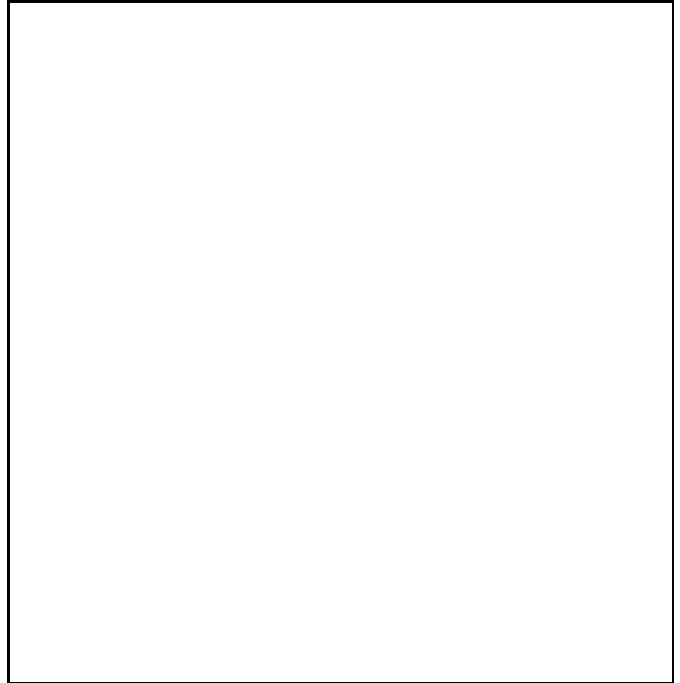


Fig. 6. a) Galaxy density as a function of the comoving distance: distance shells have been chosen in order to have a number of expected object ≥ 150 ; error bars represent 1σ Poissonian uncertainties. The solid straight line corresponds to the mean value \bar{n} , dashed lines represent 1σ uncertainties. The values refer to galaxies with $M_{b_J} \leq -12.4 + 5 \log h$, in the case of a fit with a Schechter function. b) Comoving distance histogram of ESP galaxies: the solid line is the distribution expected for a uniform sample.

Fig.5 shows the estimated average density as a function of the maximum distance for the four DH82 estimators: the values refer to galaxies with $M_{b_J} \leq -12.4 + 5 \log h$, in the case of a fit with a Schechter function. The relative behaviour of the curves does not change with other choices for M_{min} or for the case of the fit with a Schechter function and a power law. The n_3 estimator produces a very stable value for the galaxy density for all comoving distances $\gtrsim 400 h^{-1}$ Mpc, even for distances larger than the maximum distance in the sample. The difference between the maximum and minimum values of the n_3 estimator for $D_{com} > 400 h^{-1}$ Mpc is of the order of 6%, well below the 20% uncertainty due to the errors on α and M^* . All the other estimators appear to be much more sensitive to local fluctuations and vary significantly with the assumed maximum distance. For example, the density resulting from the n_{J_3} estimator would change by $\sim 25\%$ by changing the maximum distance from $\sim 650 h^{-1}$ Mpc, within which $\sim 99\%$ of our galaxies are contained, to $\sim 780 h^{-1}$ Mpc, which corresponds to the maximum distance in the sample. Since an optimal choice for the maximum distance to adopt in this analysis is not defined, this result shows an intrinsic ambiguity, at least for our sample, connected to

the n_{J_3} estimator. On the basis of this figure we therefore decided to adopt the n_3 estimator, which corresponds to a constant weighting function in eq.(13). The same estimator has been used in recent analyses of other redshift surveys, such as the LCRS (Lin et al. 1996) and the SSRS2 (Marzke & da Costa 1997). The errors on \bar{n} are computed applying the error propagation on eq.(13), taking into account also the uncertainties arising by varying α and M^* along their confidence ellipse.

The derived densities need to be corrected for the redshift incompleteness of our survey: indeed, among the 4487 objects of the photometric catalogue, we have 208 failed spectra with low signal to noise ratio and 443 not observed objects (see paper I and Sect.4.4). We assume that the failed spectra correspond to galaxies, because stars, being point-like objects, have on average a better signal to noise ratio than galaxies, and that the percentage of stars in not observed objects spectra is the same as in the spectroscopic sample (i.e. $\sim 12.2\%$). After subtracting the expected stellar contamination, we are left with about 600 not observed galaxies, corresponding to $\sim 15\%$ of the total. Therefore the galaxy counts are multiplied by the factor 1.15, before deriving the mean density. The use of a simple multiplicative factor implicitly assumes that the distance distribution of non observed galaxies is the same as that of the whole sample. This assumption is supported by the analysis of the magnitude distributions discussed in Sect.4.3.

Finally, from the estimated \bar{n} , it is possible to derive the normalization of the luminosity function as

$$\phi^* = \frac{\bar{n}}{\Gamma\left(\alpha + 1, \frac{L_1}{L^*}\right)} \quad (15)$$

in the case of a single Schechter function, and as

$$\phi^* = \frac{\bar{n}}{\Gamma\left(\alpha + 1, \frac{L_c}{L^*}\right) + \left(\frac{L_c}{L^*}\right)^{\alpha-\beta} e^{-L_c/L^*} \int_{L_1}^{L_c} \left(\frac{L}{L^*}\right)^\beta d\left(\frac{L}{L^*}\right)} \quad (16)$$

in the case of Schechter function and power law.

5.2. The results

The density radial profile of ESP galaxies is shown in Fig.6a as a function of comoving distance. In each distance bin the density has been computed using the n_3 estimator as discussed above; the error bars represent 1σ Poissonian uncertainties. The width of the various distance shells (see horizontal lines in the figure) has been chosen in order to have ~ 150 expected galaxies in each bin. The solid line represents the value of the global \bar{n} derived from the total sample (see Fig.5) and the dashed lines indicate the $\pm 1\sigma$ uncertainty on this value. The median of the \bar{n} values in the shells is $0.29 \pm 0.04 h^3 \text{ Mpc}^{-3}$, in excellent agreement with the global value $\bar{n} = 0.28 \pm 0.05 h^3 \text{ Mpc}^{-3}$.

Although the densities derived from most of the distance shells are within $\pm 2\sigma$ from the global mean density of the sample, at least three regions have densities which differ significantly (\gtrsim a factor of two) from the mean density. These regions (two underdense regions at $D_{com} \leq 140 h^{-1} \text{ Mpc}$ and $D_{com} \sim 230 h^{-1} \text{ Mpc}$, and an overdense region at $D_{com} \sim 290 h^{-1} \text{ Mpc}$) are clearly visible also in Fig.6b, which shows the observed distance histogram and the distribution expected for a uniform sample. The relatively large density fluctuations seen in our data are clearly due to the fact that our survey is a slice with a narrow width in one direction. Note, however, that over-densities and under-densities of about a factor two are seen also in wider angle surveys, such as the SSRS2 (Marzke & da Costa 1997), the CfA2 (Marzke et al. 1994) and the LCRS (Lin et al. 1996) surveys.

The results shown in this Fig.6a refer to the case of a fit with a single Schechter function for galaxies brighter than $M_{b_j} = -12.4 + 5 \log h$. Qualitatively, the results for different limiting absolute magnitudes or for the case of the fit with a Schechter function and a power law are similar to those shown in Fig.6a, except for different normalizations. The galaxy number density for $M_{b_j} \leq -16 + 5 \log h$ is well determined ($\bar{n} = 0.08 \pm 0.015 h^3 \text{ Mpc}^{-3}$) and is essentially independent from the adopted fitting law for the luminosity function. Its estimate for $M_{b_j} \leq -12.4 + 5 \log h$ is more uncertain, ranging from $\bar{n} = 0.28 \pm 0.05 h^3 \text{ Mpc}^{-3}$, in the case of a fit with a single Schechter function, to $\bar{n} = 0.54 \pm 0.10 h^3 \text{ Mpc}^{-3}$, in the case of a fit with a Schechter function and a power law. The corresponding luminosity densities in these three cases are $\rho_{LUM} = (2.0, 2.2, 2.3) \times 10^8 h L_\odot \text{ Mpc}^{-3}$, respectively: the similarity of these values indicates that the galaxies in the faint end of the luminosity function contribute strongly to the *number* density, but change only slightly the global *luminosity* density.

From these number densities we have then derived ϕ^* for the various cases: the obtained values are reported in Table 1, in the case of $M_{min} = -12.4 + 5 \log h$; the values do not change with other choices for M_{min} .

6. Discussion and comparison with previous results

In Table 2 we list the parameters from the most recent luminosity function determinations available in the literature. From this table it is clear that there are significant differences between the various surveys. We first note the discrepant value of M^* found in the CfA2 survey (Marzke et al. 1994) with respect to all the other samples, which cannot be entirely explained by the different passband used. The α and M^* parameters derived from the SSRS2 survey (Marzke & da Costa 1997) are in good agreement with our results. However, the amplitude of the SSRS2 luminosity function is such that the ratio between the SSRS2 and the ESP luminosity functions is in the range $0.4 - 0.5$

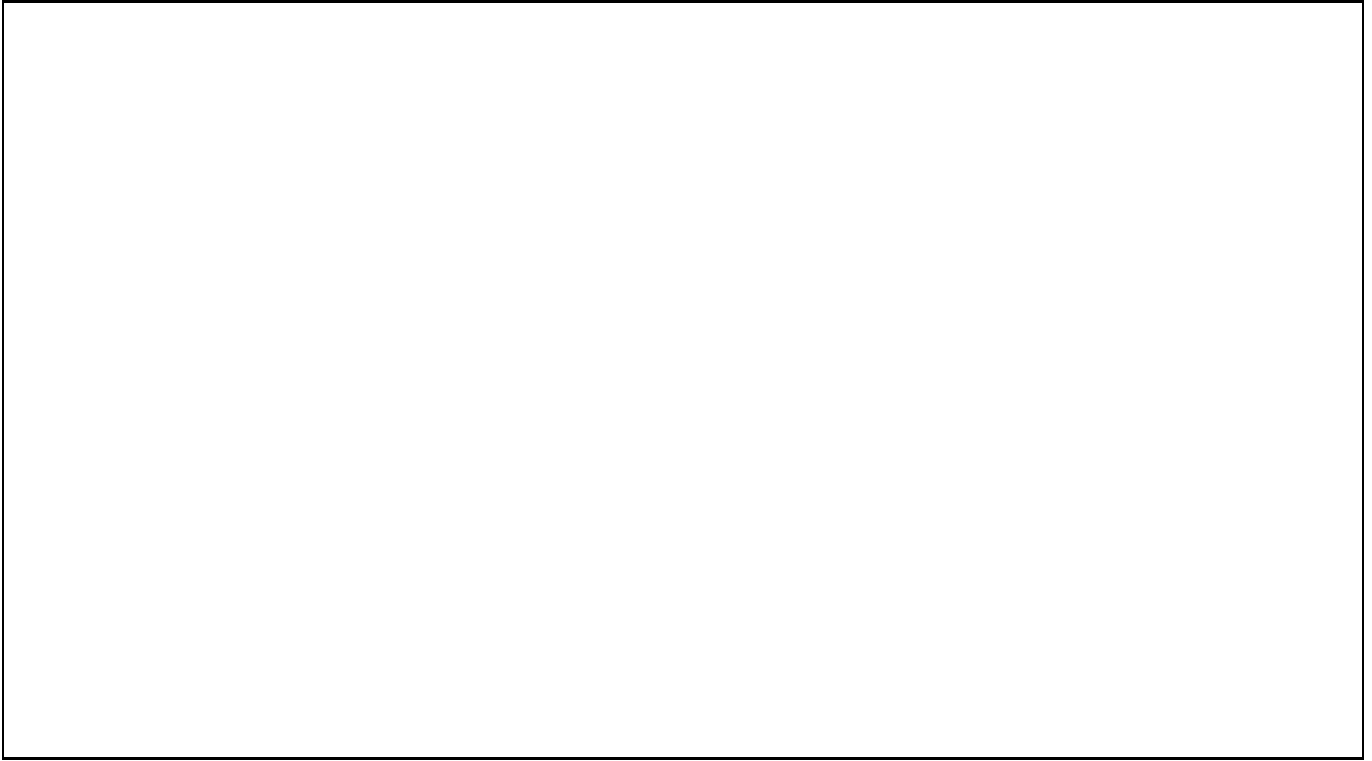


Fig. 7. a) Comparison of the ESP luminosity function with previous results. b) Ratio between the ESP luminosity function and the others. In this panel, in order to be consistent with the other luminosity functions, we have used for the ESP galaxies the fit obtained with a single Schechter function. The dotted straight lines represent an approximate $\pm 2\sigma$ uncertainty on the ratio derived from the uncertainties on the normalizations of the various surveys. For sake of clarity, the two shallow surveys (CfA2 and SSRS2) are not plotted.

Table 2. Parameters of the luminosity function from various samples

Sample	N_{gal}	m_{lim}	M_{min}	α	M^*	$\phi^* (h^3 \text{ Mpc}^{-3})$	notes
ESP	3342	$b_J = 19.4$	-12.4	$-1.22^{+0.06}_{-0.07}$	$-19.61^{+0.06}_{-0.08}$	0.020 ± 0.004	
CfA2	9063	$m_Z = 15.5$	-16.5	-1.0 ± 0.2	-18.8 ± 0.3	0.04 ± 0.01	
SSRS2	3288	$m_{B(0)} = 15.5$	-14	$-1.16^{+0.08}_{-0.06}$	-19.45 ± 0.08	0.0109 ± 0.0030	
Stromlo-APM	1658	$b_J = 17.15$	-15	-0.97 ± 0.15	-19.50 ± 0.13	0.0140 ± 0.0017	
LCRS	18678	$r \sim 17.5$	-17.5	-0.70 ± 0.05	-20.29 ± 0.02	0.019 ± 0.001	$\langle b_J - r \rangle_o = 1.1$
AUTOFIBa	588	$b_J = 24$	-14	$-1.16^{+0.05}_{-0.05}$	$-19.30^{+0.15}_{-0.12}$	$0.0245^{+0.0037}_{-0.0031}$	$0.02 < z < 0.15$
AUTOFIBb	665	$b_J = 24$	-16	$-1.41^{+0.12}_{-0.07}$	$-19.65^{+0.12}_{-0.10}$	$0.0148^{+0.0030}_{-0.0019}$	$0.15 < z < 0.35$

for $-20 < M < -14$.

In Fig.7a we compare the luminosity functions derived from the various surveys; in order to better visualize the differences, we show in Fig.7b the ratio between the ESP luminosity function and the others.

From this figure we find that:

i) The AUTOFIB luminosity functions (Ellis et al. 1996) in their first two redshift bins, which cover approximately the same distance range as our survey, are in good agreement with the ESP luminosity function. Both AUTOFIB luminosity functions are within 2σ from the ESP luminos-

ity function at all magnitudes.

ii) The Stromlo-APM (Loveday et al. 1992) and the LCRS (Lin et al. 1996) luminosity functions are significantly different from the ESP luminosity function in both shape (both are flatter than the ESP at low luminosity) and amplitude (both have a lower amplitude by a factor ~ 1.6 at $M \sim M^*$).

While a possible explanation for the difference in amplitude with respect to the Stromlo-APM luminosity function is presented later in this section, we are intrigued by the significant difference in amplitude with the LCRS lu-

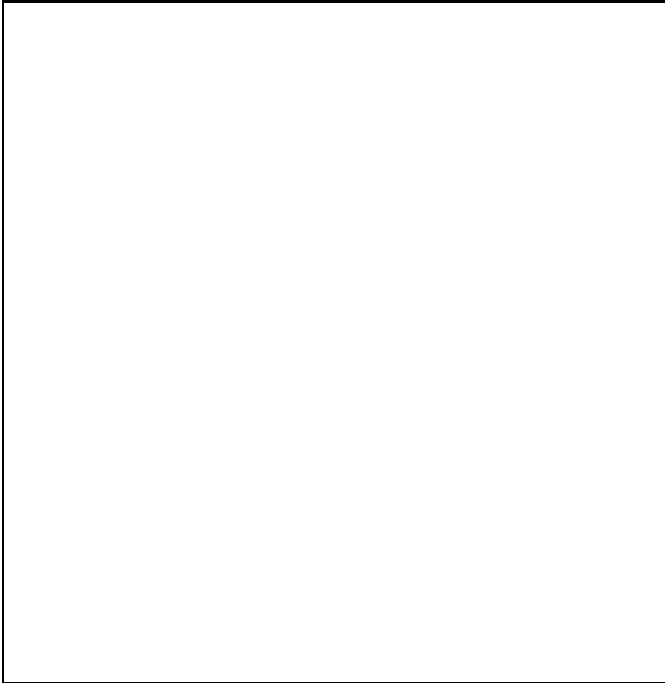


Fig. 8. Observed galaxy counts compared with those expected from the luminosity function (solid line); the same but taking into account the observed radial density variations (dashed line)

minosity function, which is derived from galaxies with a redshift distribution very similar to ours. The fact that the LCRS galaxies are selected in the red band can in principle explain, at least in part, their flatter luminosity function on the basis of the fact that at low luminosity most of the galaxies have emission lines (see Sect.4.2 above) and are presumably bluer than the average. The dependence of the local luminosity function on color has been recently discussed by Marzke & da Costa (1997), who indeed found a significantly steeper slope for blue galaxies with respect to the red ones in the SSRS2. This, however, should not affect significantly the amplitude at $M \sim M^*$. It is true that in the LCRS low surface brightness galaxies have been explicitly eliminated from the redshift survey, and therefore from the computation of the luminosity function, but the fraction of galaxies eliminated because of this selection effect is estimated to be less than 10% (Lin et al. 1996). An other difference between the LCRS and the ESP surveys is in the fraction of stars in the spectroscopic sample of candidate galaxies ($\sim 3\%$ in LCRS and $\sim 12\%$ in ESP). This can in principle be due to a better star–galaxy separation in the Las Campanas photometric data. Alternatively, it is possible that a non negligible number of galaxies, probably the most compact ones, have been classified as stars in the Las Campanas data and therefore have not been observed spectroscopically. Obviously, we have no way to check if something like this has really happened in the Las Campanas data.

We have used our derived luminosity function to compute the expected galaxy counts in the case of a constant density and compared this prediction (solid line in Fig.8) with the data in our photometric catalogue (solid circles with error bars in the same figure). Note that in this magnitude range ($b_J \leq 20$) the counts predicted using the two different fits (single Schechter function or Schechter function and power law) are almost identical, while they differ significantly at magnitudes fainter than $b_J \sim 25$.

It is clear from the figure that, while the counts predicted from the luminosity function are reasonably consistent with the data for $b_J \gtrsim 17$, they are significantly higher at brighter magnitude. Since our counts, although with large statistical errors because of the small area, are consistent with the global EDSGC (Heydon–Dumbleton et al. 1989) counts and the APM counts are consistent with the EDSGC ones (Maddox et al. 1990), this effect is essentially the same which has led Maddox et al. (1990) to suggest rapid and dramatic evolution in the galaxy properties for $z \lesssim 0.2$. Such a strong “local” evolution is not seen neither in our analysis of the luminosity function in three distance intervals (see Sect.4.2) nor in the deeper AUTOFIB redshift survey from which very little, if any, evolution is seen up to $z = 0.35$.

It has been suggested that the low APM counts at bright magnitude may be due to a magnitude scale error in the Stromlo-APM galaxy survey (Metcalfe et al. 1995). The possible existence of such an error for the APM and similar catalogues is reinforced by the recent analysis of well calibrated Schmidt plates digitized with the MAMA machine by Bertin and Dennefeld (1997). We can not exclude a similar problem in our data, although the admittedly limited CCD photometry we have obtained on bright galaxies in this area (Garilli et al. in preparation) does not show any strong magnitude error for galaxies in the magnitude range 16 – 17.

At least for our data, however, an alternative or additional interpretation is suggested by Fig.6, which shows significant fluctuations around the mean density. The dashed line in Fig.8 shows the expected counts computed by relaxing the assumption of constant density and allowing the normalization of the luminosity function to change with distance as indicated by the data points in Fig.6. In this way the agreement between the predicted and observed counts is more than acceptable over the entire magnitude range. In particular, the deficiency of the observed counts at bright magnitudes would be due to the “local” ($D_{com} \leq 140 h^{-1} \text{ Mpc}$) under-density. In this respect, it is interesting to note that, as mentioned above, the amplitude of the ESP luminosity function is about a factor of two higher than the SSRS2 one, which has been derived from galaxies with $D_{com} \lesssim 140 h^{-1} \text{ Mpc}$ over a much larger area, which includes the region of our survey. Moreover, an under-density over a similar distance range is seen also in the South Galactic Cap part of the LCRS (see Fig.8a and 8c in Lin et al. 1996). Since the LCRS

is based on galaxies extracted from a much larger area (80×6.5 sq.deg.), over which our survey region is fully contained, we are led to conclude that the local under-density seen in our data may have a size of more than $100 h^{-1}$ Mpc in at least the right ascension direction. If such an under-density extends with a similar size also in the declination direction, it could contribute significantly, possibly in addition to magnitude scale errors, to the low APM counts of bright galaxies.

In this framework, the difference in amplitude between our luminosity function and the Loveday et al. (1992) luminosity function based on APM galaxies with $b_J \leq 17.15$ could be at least partly explained by the presence of a real, giant under-density extending over a significant fraction of their survey. If we compute a luminosity function with our data but with the same limiting magnitude as in Loveday et al., the parameters we derive are fully consistent in both shape and amplitude with those derived by them. It has to be stressed, however, that the possibility for such an explanation has been considered by Loveday et al., but they did not find any evidence for it in their data (see, for example, their Fig.4).

It is also interesting to note that, since a strong “local” evolution is not easily accommodated in the standard evolutionary galaxy models, most models for the faint galaxy counts have often assumed a high normalization of the local luminosity function (see for example Guiderdoni & Rocca-Volmerange 1990, Pozzetti et al. 1996). We find that the normalization of our luminosity function is in good agreement with that usually assumed in these models and therefore our result gives an *a posteriori* confirmation of the somewhat *ad hoc* assumption adopted in these models.

7. Conclusions

In this paper we have derived the luminosity function and the mean density from the ESP galaxy redshift survey; our main results are the following:

1) Although a Schechter function is an acceptable representation of the luminosity function over the entire range of magnitudes ($M_{b_J} \leq -12.4 + 5 \log h$), our data suggest the presence of a steepening of the luminosity function for $M_{b_J} \geq -17 + 5 \log h$. Such a steepening, well fitted by a power law with slope $\beta \sim -1.6$, is in agreement with what has been recently found by similar analyses for both field galaxies (Marzke et al. 1994) and galaxies in clusters (see for instance Driver & Phillipps 1996).

2) The steepening at the faint end of the luminosity function is almost completely due to galaxies with emission lines: in fact, dividing our galaxies into two samples, i.e. galaxies with and without emission lines, we find significant differences in their luminosity functions. In particular, galaxies with emission lines show a significantly steeper slope and a fainter M^* . The volume density of galaxies with emission lines is lower than the volume den-

sity of galaxies without emission lines at bright magnitudes, but becomes higher at faint magnitudes.

3) The amplitude and the α and M^* parameters of our luminosity function are in good agreement with those of the AUTOFIB redshift survey. Viceversa, our amplitude is a factor ~ 1.6 higher, at $M \sim M^*$, than that found for both the Stromlo-APM and the Las Campanas redshift surveys. Also the faint end slope of the luminosity function is significantly steeper for the ESP galaxies than that found in these two surveys.

4) We find evidence for a local under-density, extending up to a comoving distance $\sim 140 h^{-1}$ Mpc. The volume probed by the ESP within such a distance is smaller than the volume of a typical void with $50 h^{-1}$ Mpc diameter, and in principle this observed nearby under-density could be due to the specific direction of the survey piercing through a local void. Our data do not allow to characterize this low density region in terms of size and shape. When the radial density variations observed in our data are taken into account, our derived luminosity function reproduces very well the observed counts for $b_J \leq 19.4$, including the steeper than Euclidean slope for $b_J \leq 17.0$. If this under-density extends over a much larger solid angle than that covered by our survey, it could, at least partly, explain the low amplitude of the Stromlo-APM luminosity function.

5) A similar explanation can not justify the significant difference in amplitude between the ESP and the LCRS luminosity functions, because the two samples cover essentially the same redshift range. One possibility, which has however to be verified, is that a non negligible number of galaxies are missing from the original CCD photometric catalog of the LCRS.

Given the large number of galaxies, the high degree of completeness, the accurate selection criteria and the good photometry of the ESP redshift survey, we can conclude that the results of our analysis give the best available estimate of both the normalization and the faint end slope of the luminosity function in the local Universe.

Acknowledgements. This work has been partially supported through NATO Grant CRG 920150, EEC Contract ERB-CHRX-CT92-0033, CNR Contract 95.01099.CT02 and by Institut National des Sciences de l’Univers and Cosmology GDR. We warmly thank Lucia Pozzetti for her help with the weighted K-corrections discussed in Sect.3. We thank the referee for useful comments.

References

- Avni, Y., 1976, ApJ 210, 642
- Bardelli, S., Zucca, E., Vettolani, G., Zamorani, G., 1991, A&A 248, 354
- Bertin, E., Dennefeld, M., 1997, A&A 317, 43
- Bruzual, G., Charlot, S., 1993, ApJ 405, 538
- da Costa, L.N., Geller, M.J., Pellegrini, P.S., Latham, D.W., Fairall, A.P., Marzke, R.O., Willmer, C.N.A., Huchra, J.P.,

- Calderon, J.H., Ramella, M., Kurtz, M.J., 1994, ApJ 424, L1
- Davis, M., Huchra, J.P., 1982, ApJ 254, 437 [DH82]
- Driver, S.P., Phillipps, S., 1996, ApJ 469, 529
- Efstathiou, G., Ellis, R.S., Peterson, B.A., 1988, MNRAS 232, 431
- Ellis, R.S., Colless, M., Broadhurst, T., Heyl, J., Glazebrook, K., 1996, MNRAS 280, 235
- Felenbok, P., Guerin, J., Fernandez, A., Cayatte, V., Balkowski, C., Kraan–Korteweg, R.C., 1997, *Experimental Astronomy*, in press
- Fong, R., Jones, L.R., Shanks, T., Stevenson, P.R.F., Strong, A.W., Dawe, J.A., Murray, J.D., 1987, MNRAS 224, 1059
- Guiderdoni, B., Rocca–Volmerange, B., 1990, A&A 227, 362
- Heydon–Dumbleton, N.H., Collins, C.A., MacGillivray, H.T., 1988, in *Large–Scale Structures in the Universe*, ed. W. Seitter, H.W. Duerbeck and M. Tacke (Springer–Verlag), p. 71
- Heydon–Dumbleton, N.H., Collins, C.A., MacGillivray, H.T., 1989, MNRAS 238, 379
- Lin, H., Kirshner, R.P., Shectman, S.A., Landy, S.D., Oemler, A., Tucker, D.L., Schechter, P.L., 1996, ApJ 464, 60
- Lilly, S.J., Tresse, L., Hammer, F., Crampton, D., Le Fevre, O., 1995, ApJ 455, 108
- Loveday, J., Peterson, B.A., Efstathiou, G., Maddox, S.J., 1992, ApJ 390, 338
- Lund, G., 1986, OPTOPUS – ESO Operating Manual No. 6, ESO, Garching bei München
- Lynden–Bell, D., 1971, MNRAS 155, 95
- Maddox, S.J., Sutherland, W.J., Efstathiou, G.P., Loveday, J., Peterson, B.A., 1990, MNRAS 247, 1p
- Marzke, R.O., da Costa, L.N., 1997, AJ 113, 185
- Marzke, R.O., Huchra, J.P., Geller, M.J., 1994, ApJ 428, 43
- Mattig, W., 1958, Astron. Nachr. 284, 109
- Metcalfe, N., Fong, R., Shanks, T., 1995, MNRAS 274, 769
- Pozzetti, L., Bruzual, G., Zamorani, G., 1996, MNRAS 281, 953
- Sandage, A., Tamman, G., Yahil, A., 1979, ApJ 232, 252
- Schechter, P., 1976, ApJ 203, 297
- Shanks, T., Stevenson, P.R.F., Fong, R., MacGillivray, H.T., 1984, MNRAS 206, 767
- Shectman, S.A., Landy, S.D., Oemler, A., Tucker, D.L., Lin, H., Kirshner, R.P., Schechter, P.L., 1996, ApJ 470, 172
- Vettolani, G., et al. 1992, in *International Symposium on Observational Cosmology*, G.Chincarini et al. eds., ASP conference series vol.51, p.74
- Vettolani, G., et al. 1997a, A&A in press [paper I]
- Vettolani, G., et al. 1997b, A&A to be submitted [paper III]
- Zucca, E., Pozzetti, L., Zamorani, G., 1994, MNRAS 269, 953

